

Sharp enhancement of spin fluctuations by nematic order in iron pnictides

Qiang Zhang,^{1,2} Rafael M. Fernandes,³ Jagat Lamsal,^{1,2} Jiaqiang Yan,⁴ Songxue Chi,⁴ Gregory S. Tucker,^{1,2} Daniel K. Pratt,⁵ Jeffrey W. Lynn,⁵ R. W. McCallum,^{1,6} Paul C. Canfield,^{1,2} Thomas A. Lograsso,^{1,6} Alan I. Goldman,^{1,2} David Vaknin,^{1,2} and Robert J. McQueeney^{1,2,4,*}

¹Ames Laboratory, Ames, IA, 50011, USA

²Department of Physics and Astronomy, Iowa State University, Ames, IA, 50011, USA

³School of Physics and Astronomy, University of Minnesota, Minneapolis, MN 55455, USA

⁴Oak Ridge National Laboratory, Oak Ridge, Tennessee 37831, USA

⁵NIST Center for Neutron Research, National Institute of Standards and Technology, Gaithersburg, Maryland 20899-6102, USA

⁶Department of Materials Sciences and Engineering, Iowa State University, Ames, Iowa 50011, USA

(Dated: December 7, 2024)

Inelastic neutron scattering was employed to investigate the impact of electronic nematic order on the magnetic spectra of LaFeAsO and Ba(Fe_{0.953}Co_{0.047})₂As₂. These materials are ideal to study the paramagnetic-nematic state, since the nematic order, signaled by the tetragonal-to-orthorhombic transition at T_S , sets in well above the stripe antiferromagnetic ordering at T_N . We find that the temperature-dependent dynamic susceptibility displays an anomaly at T_S followed by a sharp enhancement in the spin-spin correlation length, revealing a strong feedback effect of nematic order on the low-energy magnetic spectrum. Our findings can be consistently described by a model that attributes the structural/nematic transition to magnetic fluctuations, and unveils the key role played by nematic order in promoting the long-range stripe antiferromagnetic order in iron pnictides.

One of the most interesting features of the “122” (e.g. BaFe₂As₂) and “1111” (e.g. LaFeAsO) families of iron-based superconductors is the intimate coupling between superconductivity (SC), stripe antiferromagnetic order (AFM), and the tetragonal-to-orthorhombic structural transition [1–5]. For example, in both families, chemical substitutions on the transition metal site, such as Co and Ni, suppress the AFM ordering and the structural transition and, over a limited range of doping, promote SC [4]. For underdoped BaFe₂As₂, evidence of a direct competition between AFM and SC has been presented [6–10] in addition to a suppression of the orthorhombic distortion below the superconducting transition temperature T_C [11, 12]. Despite this competition between SC and long-range magnetic/orthorhombic order, SC generally arises when large AFM/structural fluctuations are present [13], a feature that attests the intricate relationship between these three intertwined phases [14].

While these previous studies have focused on the impact of SC on the magnetic and orthorhombic phases, the interplay between these two ordered states has been a topic of intense debate [15]. For the parent compounds of the “122” family, the magnetic transition temperature (T_N) practically coincides with the structural distortion at T_S [16–18], whereas in the Co-underdoped BaFe₂As₂ and in the parent compounds of the “1111” family, such as LaFeAsO, the orthorhombic distortion occurs well above T_N [19, 20]. The structural transition has been proposed to be driven by electronic correlations [21] – associated with either spin [22–26] or charge/orbital degrees of freedom [27–30] – giving rise to the so-called nematic phase in the temperature range between T_S and T_N . This electronic nematic phase is characterized not only by a weak in-plane structural anisotropy manifested by

distinct a and b lattice constants [11], but also by large in-plane anisotropies in many electronic properties, such as resistivity [21, 31, 32], optical conductivity [33–35], thermopower [36], uniform susceptibility [37, 38], and charge correlations [19, 39, 40]. Previous ARPES [41–44], STM [45, 46], and Raman [47] studies focused on how nematic order affects the normal-state electronic spectrum and, in particular, the charge and orbital degrees of freedom. However, little is known about how nematic order affects the low-energy magnetic fluctuations [48–52], which are particularly important for the formation of the SC state [13].

Here we perform inelastic neutron scattering (INS) experiments to elucidate the evolution of the magnetic spectrum across the nematic transition in single crystals of LaFeAsO and Ba(Fe_{0.953}Co_{0.047})₂As₂, focusing on the behaviors of the imaginary part of the dynamic magnetic susceptibility $\chi''(\mathbf{Q}, E)$ and of the spin-spin correlation length ξ as a function of temperature. These two systems exhibit an orthorhombic distortion whose onset is well separated from the stripe AFM ordering [6, 19, 53, 54], enabling the survival of the nematic phase over a considerable temperature range. Our measurements in twinned samples find clear anomalies in the magnetic spectrum at T_S . In particular, we find that not only is the overall low-energy magnetic intensity enhanced below T_S , but also that the spin-spin correlation length undergoes a sharp increase at the nematic transition temperature, in contrast with what one expects from a common AFM system. This effect reveals a cooperative relationship between nematicity and magnetism, in agreement with theoretical predictions from models that attribute the nematic transition to a spontaneous symmetry breaking driven by magnetic fluctuations [22–26].

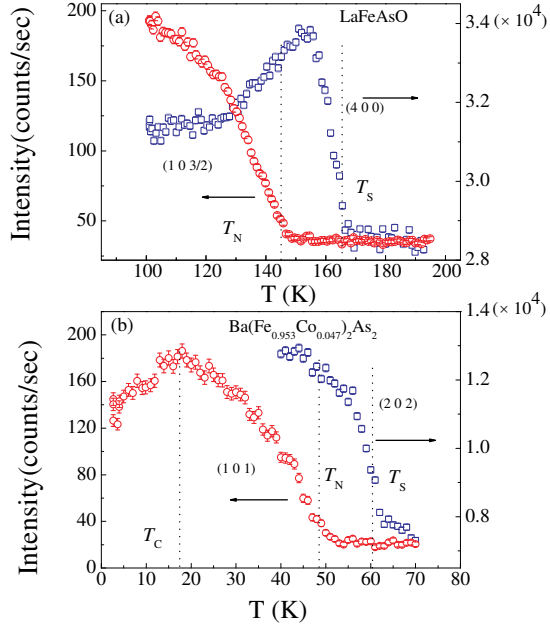


FIG. 1: (color online) (a) Neutron diffraction peak intensities of the $(1\ 0\ 3/2)$ magnetic reflection and the $(4\ 0\ 0)/(0\ 4\ 0)$ Bragg reflection as a function of temperature in LaFeAsO. (b) Neutron diffraction peak intensities of the $(1\ 0\ 1)$ magnetic reflection and the $(2\ 0\ 2)/(0\ 2\ 2)$ Bragg reflection as a function of temperature in Ba(Fe_{0.953}Co_{0.047})₂As₂.

The LaFeAsO and Ba(Fe_{0.953}Co_{0.047})₂As₂ crystals were grown using a flux technique as previously described[53, 54]. Dozens of small single-crystals of LaFeAsO with a total mass of approximately 600 mg were co-aligned at the (HOL) plane within ~ 2 degrees mosaicity. Hereafter, unless otherwise noted with a subscript “T”, we use orthorhombic notation. A large single crystal of Ba(Fe_{0.953}Co_{0.047})₂As₂ with a mass of ≈ 700 mg was also aligned in (HOL) for the investigation. The elastic and inelastic neutron measurements on LaFeAsO and Ba(Fe_{0.953}Co_{0.047})₂As₂ were performed on the HB3 spectrometer (located at the High Flux Isotope Reactor at Oak Ridge National Laboratory) and BT-7 triple-axis neutron spectrometer at the NIST Center for Neutron Research [55], respectively.

In LaFeAsO, neutron diffraction measurements of the $(1\ 0\ 3/2)$ magnetic Bragg reflection and the $(4\ 0\ 0)/(0\ 4\ 0)$ nuclear Bragg reflection as a function of temperature show a structural transition at $T_S=165$ K split from the magnetic transition at $T_N=145$ K, as illustrated in Fig 1 (a), and consistent with previous reports [19, 53, 56, 57]. The $(4\ 0\ 0)/(0\ 4\ 0)$ reflection, which develops from the $(2\ 2\ 0)_T$ tetragonal Bragg reflection, was used to monitor the structural transition indirectly by virtue of secondary extinction changes resulting from the structural transition. Similarly, in Ba(Fe_{0.953}Co_{0.047})₂As₂, the intensity of the $(2\ 0\ 2)/(0\ 2\ 2)$ nuclear Bragg reflection

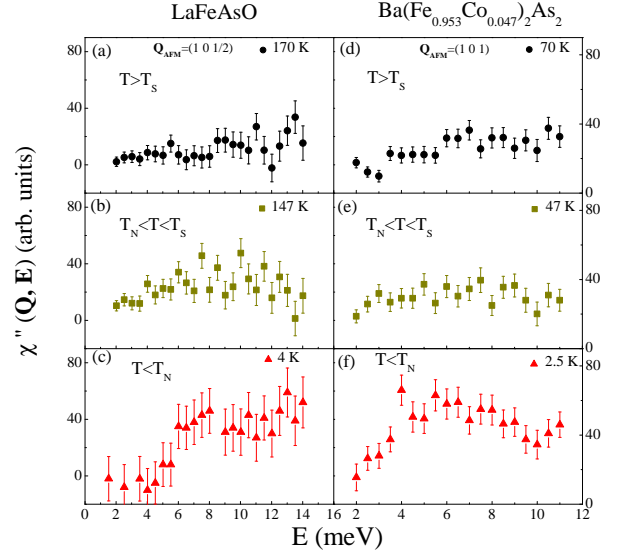


FIG. 2: (color online) Low-energy spin excitation in LaFeAsO at (a) 170 K, (b) 147 K, (c) 4 K and in Ba(Fe_{0.953}Co_{0.047})₂As₂ at (d) 70 K, (e) 47 K, (f) 2.5 K. The results are derived from the difference between a constant-Q energy scan at \mathbf{Q}_{AFM} and a background scan at $\mathbf{Q}'=(0.7\ 0\ 1)$ for Ba(Fe_{0.953}Co_{0.047})₂As₂ and at $\mathbf{Q}'=(0.83\ 0\ 0.998)$ after the crystal was rotated from nominal \mathbf{Q}_{AFM} by 20° for LaFeAsO. The intensities have been normalized to reflect a counting time of approximately five minutes. Error bars where indicated represent one standard deviation.

indicates that the structural transition occurs at $T_S = 60$ K, which is split from the magnetic transition at $T_N = 47$ K according to the $(1\ 0\ 1)$ magnetic Bragg reflection. The anomalous decrease of the intensity of the $(1\ 0\ 1)$ magnetic peak below $T_C \approx 17$ K marks the reduction of the AFM order parameter due to competition with the SC state [6]. The locations of these three transitions in Ba(Fe_{0.953}Co_{0.047})₂As₂ are also consistent with previous reports[39, 54].

To determine the impact of nematic order on the magnetic spectrum, we explore the dependence of the imaginary part of the dynamic susceptibility $\chi''(\mathbf{Q}, E)$ on the energy E , the momentum \mathbf{Q} , and the temperature T . This quantity is extracted via the relationship:

$$S(\mathbf{Q}, E) \propto f^2(Q)\chi''(\mathbf{Q}, E)(1 - e^{-E/k_B T})^{-1} \quad (1)$$

where $S(\mathbf{Q}, E)$ is the measured background-subtracted intensity $I(\mathbf{Q}, E) - B(\mathbf{Q}', E)$, $f(Q)$ is the magnetic form factor of Fe²⁺, and k_B is the Boltzmann constant. Figure 2 shows $\chi''(\mathbf{Q}_{\text{AFM}}, E)$ at the magnetic reflection $\mathbf{Q}_{\text{AFM}}=(1\ 0\ 1/2)$ in LaFeAsO and $\mathbf{Q}_{\text{AFM}}=(1\ 0\ 1)$ in Ba(Fe_{0.953}Co_{0.047})₂As₂ at several temperatures. Below T_N , the spectra in LaFeAsO exhibit the onset of an energy gap ~ 5 meV, consistent with previous reports[56]. In Ba(Fe_{0.953}Co_{0.047})₂As₂, a heavily overdamped energy gap ~ 10 meV[58] is observed. The spin gaps in both systems vanish above T_N and the energy-dependent damping

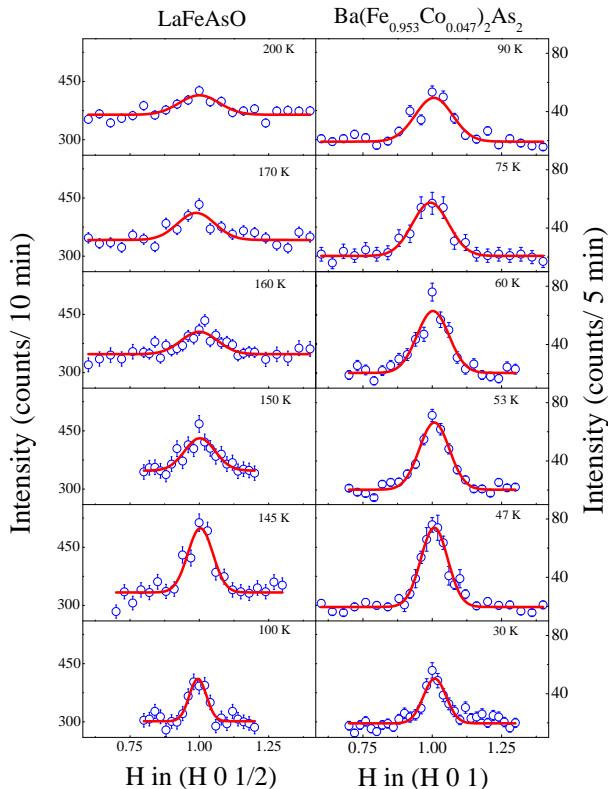


FIG. 3: (Color online) Representative longitudinal H scans (a) through $\mathbf{Q}_{\text{AFM}} = (1\ 0\ 1/2)$ at $E = 5$ meV and various temperatures in LaFeAsO and (b) through $\mathbf{Q}_{\text{AFM}} = (1\ 0\ 1)$ at $E = 3$ meV and various temperatures in Ba(Fe_{0.953}Co_{0.047})₂As₂. The solid lines are obtained by the best fit to the data to a Gaussian function.

also increases above T_N . These results guide us to measure $\chi''(\mathbf{Q}, E)$ at a fixed energy transfer of $E = 5$ meV in LaFeAsO and, $E = 3$ meV in Ba(Fe_{0.953}Co_{0.047})₂As₂ to obtain both the spin-spin correlation length and the magnetic intensity as a function of temperature, according to the model for spin fluctuations described in Ref. [58].

Representative longitudinal H scans through $\mathbf{Q}_{\text{AFM}} = (1\ 0\ 1/2)$ in LaFeAsO and $\mathbf{Q}_{\text{AFM}} = (1\ 0\ 1)$ in Ba(Fe_{0.953}Co_{0.047})₂As₂ at low energy transfers are shown in Fig. 3. The solid lines represent Gaussian fits to the data (see the Supplemental Material). We note that upon decreasing the temperature below T_S , the lineshape narrows and the peak amplitude increases. The dynamic susceptibility and linewidth (full width at half maximum) versus temperature are shown in Fig. 4. The dynamic susceptibility shows a discontinuous increase below T_S (much stronger for LaFeAsO) and exhibits a maximum at the AFM ordering temperature T_N , followed by a gradual decrease below T_N due to the opening of the spin gap. As shown in Fig. 4 (b) and (d), the linewidth decreases as T approaches T_N , which is expected for a

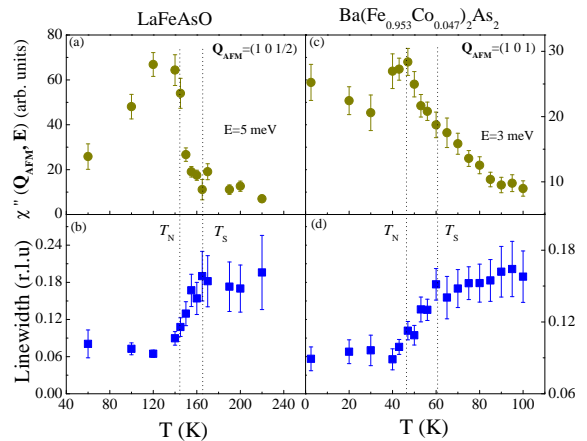


FIG. 4: (color online) Temperature dependence of (a) dynamic susceptibility $\chi''(\mathbf{Q}, E = 5$ meV) and (b) the Gaussian linewidth, obtained by fitting the longitudinal H scans through $\mathbf{Q}_{\text{AFM}} = (1\ 0\ 1/2)$ at $E = 5$ meV in LaFeAsO. Temperature dependence of (c) the dynamic susceptibility $\chi''(\mathbf{Q}, E = 3$ meV) and (d) the Gaussian linewidth, obtained by fitting the longitudinal H scans through $\mathbf{Q}_{\text{AFM}} = (1\ 0\ 1)$ at $E = 3$ meV in Ba(Fe_{0.953}Co_{0.047})₂As₂. The vertical dashed lines mark the locations of the structural transition T_S and the AFM magnetic transition T_N .

classic second-order AFM phase transition. The striking result of this study is the observation of a sharp decrease in the linewidth below T_S in both LaFeAsO and Ba(Fe_{0.953}Co_{0.047})₂As₂ systems, which signifies a strong effect of nematic order on the approach to AFM order.

Above the magnetic transition temperature T_N , the linewidth is proportional to the inverse magnetic correlation length ξ^{-1} associated with the paramagnetic fluctuations (see the justification in the Supplemental Material). Therefore, the onset of long-range nematic order promotes a strong increase of this correlation length, enhancing the tendency of the system towards long-range magnetic order. Such a cooperative interplay between nematicity and magnetism can be understood qualitatively within models that attribute the tetragonal symmetry-breaking to magnetic fluctuations emerging from either localized [22, 23] or itinerant spins [25]. To illustrate the corresponding microscopic mechanism, we show schematically in Fig. 5(a) the evolution of the magnetic fluctuations across T_S and T_N both in real space (upper panels) and in spin space (lower panels). The crucial point behind this mechanism is that the iron pnictides display two degenerate stripe AFM ground states, with ordering vectors $\mathbf{Q}_1 = (1\ 0\ L)$ and $\mathbf{Q}_2 = (0\ 1\ L)$. Thus, the magnetic ground state can be described in terms of two interpenetrating square sublattices – associated with the two distinct Fe atoms in the unit cell – that tend to order magnetically in Néel-like configurations (blue and red dashed lines in Fig. 5(a)).

Above T_S , where there is no long-range magnetic or-

der, these two sublattices are essentially independent (as shown in the upper left panel of Fig. 5(a)), and their fluctuations are uncoupled (as shown in the lower left panel). As a result, the system has multiple possible ground states, a feature commonly seen in frustrated spin systems with low magnetic transition temperatures. However, below T_S but above T_N , nematic order emerges as a coupling between the two sublattices (upper middle panel in Fig.5(a)), enforcing the two corresponding Néel order parameters to fluctuate coherently either anti-parallel (as shown in the lower middle panel) or parallel to each other. There is still no long-range magnetic order, since the spins can point at any direction in spin space. However, the tetragonal symmetry of the system is broken, since nearest-neighbor spins are locked in a ferromagnetic-like or an antiferromagnetic-like configuration. Furthermore, by breaking the tetragonal symmetry, nematic order reduces the number of possible magnetic ground states to only one – either the $\mathbf{Q}_1 = (1\ 0\ L)$ stripe if the a direction is selected along the x axis, or the $\mathbf{Q}_2 = (0\ 1\ L)$ stripe if the a direction is selected along the y direction. Thus, the frustration present at higher temperatures is lifted by nematic order, resulting in an enhancement of the spin-spin correlation length ξ , and therefore of T_N , which sets in when ξ diverges (right panels). Note that this phenomenon can be observed even in twinned samples as the ones studied here, since magnetic fluctuations are enhanced regardless of the type of nematic domain selected.

To go beyond this qualitative analysis, we calculate the spin-spin correlation length ξ^{-1} near the nematic transition within the itinerant three-band model of Ref. [25] and compare it with the experimentally measured linewidth for both LaFeAsO and $\text{Ba}(\text{Fe}_{0.953}\text{Co}_{0.047})_2\text{As}_2$ compounds. To take into account the experimental resolution of the peaks and the fact that they are measured at a non-zero energy, we shift the inverse correlation length by a temperature-independent $\delta_{\text{res}} > 0$ to model the linewidth W , $W \propto \xi^{-1} + \delta_{\text{res}}$. As shown in Fig. 5(b), our model is able to consistently describe the temperature evolution of the linewidth (solid red lines), most notably the sharp decrease of W at T_S . Extrapolation of the temperature behavior of the correlation length above T_S to lower temperatures (dashed red lines) reveals that, in the absence of the nematic transition, T_N would be expected to take place at much lower temperatures. This behavior is a hallmark of frustrated magnetic systems, confirming our interpretation that nematic order promotes long-range magnetic order. We note that the model used here is valid only in the vicinity of the structural and magnetic transitions, therefore it is not suitable to capture the behavior of the correlation length well above or below T_N .

In summary, we have reported unambiguous evidence for the feedback effect of nematic order on the magnetic spectrum in both “1111” and underdoped “122” families

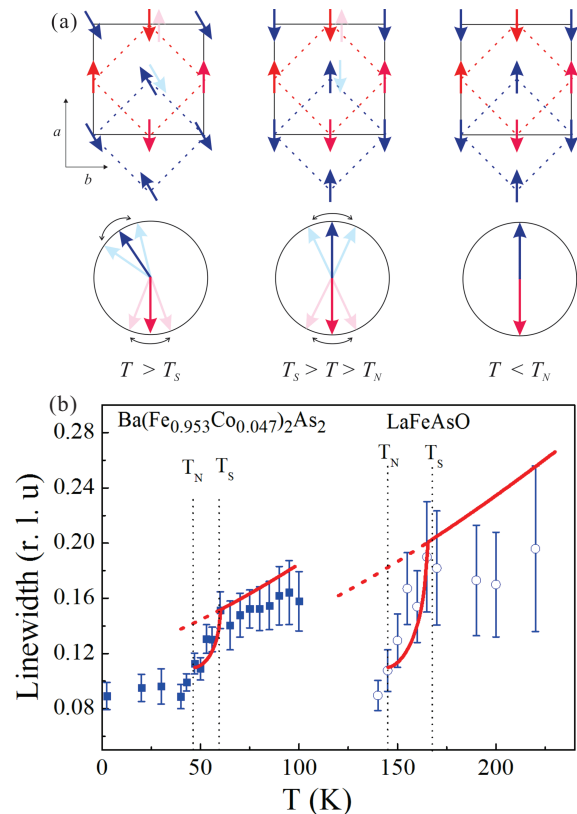


FIG. 5: (color online) (a) Evolution of the magnetic fluctuations of the iron pnictides in real space (upper panels) and spin space (lower panels). The two Néel sublattices corresponding to the two different Fe atoms of the unit cell (dashed lines) are shown in red and blue. Above T_N , spins in each sublattice fluctuate around a Néel configuration. These fluctuations are uncoupled above T_S , but below T_S , the two fluctuating Néel sublattices are coupled either parallel or anti-parallel to each other. The double arrows in the upper panels represent fluctuating spins, as explicitly shown in the lower panels. Below T_N , spins point to a fixed direction in spin space. (b) Temperature dependence of the theoretical linewidth W (red lines) compared to the experimental linewidth (blue dots). The dashed lines mark the locations of T_S and T_N in LaFeAsO and $\text{Ba}(\text{Fe}_{0.953}\text{Co}_{0.047})_2\text{As}_2$.

of the iron pnictides with $T_S > T_N$, manifested by the sharp enhancement of the spin-spin correlation length below T_S , revealing a key impact of this elusive electronic order on the normal-state properties of the iron arsenides. Since magnetic fluctuations are believed to be important for the formation of the SC state [13], and our results provide evidence that nematic order enhances them, this suggests that nematicity may be more than another competing order, as previously reported [11, 12], and may even help enhancing T_C in some circumstances [59, 60].

Acknowledgements. Research at Ames Laboratory is supported by the US Department of Energy, Office of Basic Energy Sciences, Division of Materials Sciences and Engineering under Contract No. DE-AC02-07CH11358.

R.M.F. is supported by the Department of Energy under Award Number DE-SC0012336. Use of the high flux isotope reactor at the Oak Ridge National Laboratory, was supported by the US Department of Energy, Office of Basic Energy Sciences, Scientific User Facilities Division. The NIST Center for Neutron Research is supported by the US Department of Commerce. We acknowledge Dan Parshall for his technical assistance in measuring $\text{Ba}(\text{Fe}_{0.953}\text{Co}_{0.047})_2\text{As}_2$ at BT-7 triple-axis neutron spectrometer at the NIST center for Neutron Research.

* Electronic address: mcqueeneyrj@ornl.gov

- [1] K. Ishida, Y. Nakai and H. Hosono, *J. Phys. Soc. Japan* **78**, 062001 (2009).
- [2] D. C. Johnston, *Adv. Phys.* **59**, 803 (2010)
- [3] J. Paglione and R. L. Greene, *Nature Phys.* **6**, 645 (2010)
- [4] P. C. Canfield and S. L. Bud'ko, *Annu. Rev. Cond. Mat. Phys.* **1**, 27 (2010)
- [5] H. H. Wen and S. Li, *Annu. Rev. Cond. Mat. Phys.* **2**, 121 (2011).
- [6] D. K. Pratt, W. Tian, A. Kreyssig, J. L. Zarestky, S. Nandi, N. Ni, S. L. Bud'ko, P. C. Canfield, A. I. Goldman, and R. J. McQueeney, *Phys. Rev. Lett.* **103**, 087001 (2009).
- [7] A. D. Christianson, M. D. Lumsden, S. E. Nagler, G. J. MacDougall, M. A. McGuire, A. S. Sefat, R. Jin, B. C. Sales, and D. Mandrus, *Phys. Rev. Lett.* **103**, 087002 (2009).
- [8] R. M. Fernandes *et al.*, *Phys. Rev. B* **81**, 140501(R) (2010).
- [9] S. Avci, O. Chmaissem, E. A. Goremychkin, S. Rosenkranz, J.-P. Castellan, D. Y. Chung, I. S. Todorov, J. A. Schlueter, H. Claus, M. G. Kanatzidis, A. Daoud-Aladine, D. Khalyavin, and R. Osborn, *Phys. Rev. B* **83**, 172503 (2011).
- [10] Huiqian Luo, Rui Zhang, Mark Laver, Zahra Yamani, Meng Wang, Xingye Lu, Miaoyin Wang, Yanchao Chen, Shiliang Li, Sung Chang, Jeffrey W. Lynn, and Pengcheng Dai, *Phys. Rev. Lett.* **108**, 247002 (2012).
- [11] S. Nandi *et al.*, *Phys. Rev. Lett.* **104**, 057006 (2010).
- [12] A. E. Böhrer, P. Burger, F. Hardy, T. Wolf, P. Schweiss, R. Fromknecht, H. v. Löhneysen, C. Meingast, H. K. Mak, R. Lortz, S. Kasahara, T. Terashima, T. Shibauchi, and Y. Matsuda, *Phys. Rev. B* **86**, 094521 (2012).
- [13] P. J. Hirschfeld, M. M. Korshunov, and I. I. Mazin, *Rep. Prog. Phys.* **74**, 124508 (2011); A. V. Chubukov, *Annu. Rev. Cond. Mat. Phys.* **3**, 57 (2012).
- [14] E. Fradkin, S. A. Kivelson, and J. M. Tranquada, arXiv:1407.4480 (2014).
- [15] R. M. Fernandes, A. V. Chubukov, and J. Schmalian, *Nature Phys.* **10**, 97 (2014).
- [16] H.-F. Li, *et al.*, *Phys. Rev. B* **80**, 054407 (2009).
- [17] M. G. Kim, *et al.*, *Phys. Rev. B* **83**, 134522 (2011).
- [18] C. R. Rotundu and R. J. Birgeneau, *Phys. Rev. B* **84**, 092501 (2011).
- [19] H.-F. Li, *et al.*, *Phys. Rev. B* **82**, 064409 (2010).
- [20] Q. Zhang, *et al.*, *Phys. Rev. B* **88**, 174517 (2013).
- [21] J.-H. Chu, H.-H. Kuo, J. G. Analytis, and I. R. Fisher, *Science* **337**, 710 (2012).
- [22] C. Fang, H. Yao, W.-F. Tsai, J. Hu, and S. A. Kivelson, *Phys. Rev. B* **77**, 224509 (2008).
- [23] C. Xu, M. Muller, and S. Sachdev, *Phys. Rev. B* **78**, 020501 (2008).
- [24] R. M. Fernandes, *et al.*, *Phys. Rev. Lett.* **105**, 157003 (2010).
- [25] R. M. Fernandes, A. V. Chubukov, J. Knolle, I. Eremin, and J. Schmalian, *Phys. Rev. B* **85**, 024534 (2011).
- [26] S. Liang, A. Moreo, and E. Dagotto, *Phys. Rev. Lett.* **111**, 047004 (2013).
- [27] C. C. Lee, W. G. Yin, and W. Ku, *Phys. Rev. Lett.* **103**, 267001 (2009).
- [28] C.-C. Chen, J. Maciejko, A. P. Sorini, B. Moritz, R. R. P. Singh, and T. P. Devereaux, *Phys. Rev. B* **82**, 100504 (2010).
- [29] W.-C. Lee and P. W. Phillips, *Phys. Rev. B* **86**, 245113 (2012).
- [30] S. Onari H. and Kontani, *Phys. Rev. Lett.* **109**, 137001 (2012).
- [31] J.-H. Chu, *et al.*, *Science* **329**, 824 (2010).
- [32] M. A. Tanatar *et al.*, *Phys. Rev. B* **81**, 184508 (2010).
- [33] A. Dusza *et al.*, *Europhys. Lett.* **93**, 37002 (2011).
- [34] M. Nakajima *et al.*, *Proc. Natl. Acad. Sci. U.S.A.* **108**, 12238-12242 (2011).
- [35] A. Patz, *et al.*, *Nature Comm.* **5**, 3229 (2014).
- [36] S. Jiang *et al.*, *Phys. Rev. Lett.* **110**, 067001 (2013).
- [37] S. Kasahara, *et al.*, *Nature* **486**, 382 (2012).
- [38] Xiaofeng Xu *et al.*, *Phys. Rev. B* **89**, 104517 (2014).
- [39] Q. Zhang, *et al.*, *Phys. Rev. B* **87**, 094510 (2013).
- [40] Y. K. Kim *et al.*, *Phys. Rev. Lett.* **111**, 217001 (2013).
- [41] M. Yi, *et al.*, *Proc. Nat. Acad. Sci.* **108**, 6878 (2011).
- [42] Y. Zhang *et al.*, *Phys. Rev. B* **85**, 085121 (2012).
- [43] M Yi *et al.*, *New J. Phys.* **14**, 073019 (2012).
- [44] T. Shimojima *et al.*, *Phys. Rev. B* **89**, 045101 (2014).
- [45] T.-M. Chuang *et al.*, *Science* **327**, 181-184 (2010).
- [46] E. P. Rosenthal *et al.*, *Nature Phys.* **10**, 225 (2014).
- [47] Y. Gallais *et al.*, *Phys. Rev. Lett.* **111**, 267001 (2013).
- [48] L. Ma *et al.*, *Phys. Rev. B* **83**, 132501 (2011).
- [49] M. Fu *et al.*, *Phys. Rev. Lett.* **109**, 247001 (2012).
- [50] Y. Song *et al.*, *Phys. Rev. B* **88**, 134512 (2013).
- [51] H. Luo *et al.*, *Phys. Rev. Lett.* **111**, 107006 (2013).
- [52] X. Lu *et al.*, *Science* **345**, 657 (2014).
- [53] J.-Q. Yan, *et al.*, *Appl. Phys. Lett.*, **95**, 222504 (2009).
- [54] N. Ni, M. E. Tillman, J.-Q. Yan, A. Kracher, S. T. Hannahs, S. L. Bud'ko, and P. C. Canfield, *Phys. Rev. B* **78**, 214515 (2008).
- [55] J. W. Lynn, *et al.*, *Journal of Research of NIST*, **117**, 61-79 (2012).
- [56] M. Ramazanoglu, *et al.*, *Phys. Rev. B* **87**, 140509 (2013).
- [57] C. A. McElroy, *et al.*, *Phys. Rev. B* **88**, 134513 (2013).
- [58] G. S. Tucker, *et al.*, *Phys. Rev. B* **89**, 180503(R) (2014).
- [59] R. M. Fernandes and A. J. Millis, *Phys. Rev. Lett.* **111**, 127001 (2013).
- [60] F. Yang, F. Wang, and D.-H. Lee, *Phys. Rev. B* **88**, 100504 (2013).